HHS Public Access
Author manuscript
J Biomed Mater Res A. Author manuscript; available in PMC 2016 December 01.

Published in final edited form as:
J Biomed Mater Res A. 2015 December ; 103(12): 3807–3814. doi:10.1002/jbm.a.35524.

Nitric Oxide Regulates Cell Behavior on an Interactive Cell-derived Extracellular Matrix Scaffold

Qi Xing[1], **Lijun Zhang**[1,2], **Travis Redman**[1], **Shaohai Qi**[2], and **Feng Zhao**[1,*]

[1]Department of Biomedical Engineering, Michigan Technological University, 1400 Townsend Drive, Houghton, MI 49931

[2]Department of Burns, the First Affiliated Hospital of Sun Yat-sen University, Guangzhou, Guangdong, China

Abstract

During tissue injury and wound healing process, there are dynamic reciprocal interactions among cells, extracellular matrix (ECM) and mediating molecules which are crucial for functional tissue repair. Nitric oxide (NO) is one of the key mediating molecules that can positively regulate various biological activities involved in wound healing. Various ECM components serve as binding sites for cells and mediating molecules, and the interactions further stimulate cellular activities. Human mesenchymal stem cells (hMSCs) can migrate to the wound site and contribute to tissue regeneration through differentiation and paracrine signaling. The objective of this work was to investigate the regulatory effect of NO on hMSCs in an interactive ECM-rich microenvironment. In order to mimic the *in vivo* stromal environment in wound site, a cell-derived ECM scaffold that was able to release NO within the range of *in vivo* wound fluid NO level was fabricated. Results showed that the micro-molar level of NO released from the ECM scaffold had an inhibitory effect on cellular activities of hMSCs. The NO impaired cell growth, altered cell morphology, disrupted the F-actin organization, also decreased the expression of focal adhesion related molecules integrin $\alpha 5$ and paxillin. These results may contribute to the elucidation of how NO acts on hMSCs in wound healing process.

Introduction

Tissue injury and healing is a complex series of reactions and interactions at both the cellular and molecular level [1]. During the inflammation, proliferation, and remodeling phases of the wound healing process, there are dynamic, reciprocal interactions among cells, growth factors and mediating molecules, as well as extracellular matrix (ECM) [2]. One of the most important mediating molecules is nitric oxide (NO), a highly reactive and lipophilic molecule that functions in many aspects of the wound healing process; such as, inflammation mediation, matrix deposition and remodeling, cell proliferation, and angiogenesis [3]. Specifically, NO regulates signaling pathways of the anti-inflammatory cytokine secretion that are involved in tissue repair and wound healing [4]. NO stimulates collagen synthesis and keratinocyte migration, thus contributing to wound contraction and

[*]Corresponding to: Feng Zhao, fengzhao@mtu.edu, Tel: 906-487-2852, Fax: 906-487-1717.

closure [4]. NO is generated *in vivo* from L-arginine catalyzed by three types of nitric oxide synthases (NOSs) [5]. Among them, inducible NOSs (iNOSs) responds to acute inflammatory stimuli including wounding, thermal injury, and exposure to endotoxins or cytokines, which all produce large amounts of NO from immune and non-immune cells [6]. During the early inflammation phase of would healing, there is a rapid increase of NO which may peak as fast as 48 hours. The majority of NO synthesis is contributed to inflammatory cells, including neutrophils and macrophages. In the following proliferation and remodeling phases, fibroblasts and endothelial cells continue releasing NO, but the overall NO release profile can be described as a decreasing curve over time [7]. The physiological function of NO is based on its regulation of cells including cell adhesion, proliferation, migration and differentiation. Therefore, investigation of NO effect on cellular behavior *in vitro* will help to understand the mechanism of NO in tissue repair.

Nitric oxide has a short half-life, which limits its influence distance from the source to ~100 μm [8]. Furthermore, NO donors of small molecules are fairly easy to disperse into the environment rapidly. It is thus crucial to develop systems capable of local and controllable NO release for effective delivery. The small NO donors can be conjugated onto macromolecular scaffolds for spatially controlled and sustained NO release, which may provide a more efficient method to investigate the effects of NO on cell behaviors *in vitro*. A wide variety of macromolecular scaffolds, including protein, synthetic polymers, and inorganic nanoparticles, have been successfully employed to fabricate NO-releasing materials [9]. However, none of them can recapitulate the microenvironment in natural tissues. A scaffold that largely mimics the ECM components and structure of native tissues may benefit the *in vitro* investigation on the impact of NO for cellular functions.

The ECM in natural tissues plays a critical role in regulating cell behaviors such as proliferation, adhesion, migration, and differentiation [10]. The interactions between ECM and cells, and also between ECM and growth factors, are fundamental to all phases of tissue healing [2]. ECM is composed of a complex assembly of different proteins and proteoglycans which play important roles in wound healing [11]. Structural protein, collagen, is deposited at the wound site to restore tissue integrity [12]. Adhesion glycoprotein, fibronectin, mediates cell-ECM interaction and cell-cell contacts, thus promoting cell migration and adhesion to wound sites [13]. Proteoglycans maintains tissue hydration, which is critical for wound healing process [14]. In addition, degradation and remodeling of ECM by matrix metalloproteases is crucial for leukocyte influx, angiogenesis, and tissue remodeling [15]. Employment of ECM as a scaffold in an *in vitro* model system for a wound healing study would better recapitulate the naturally occurring microenvironment. A cell-derived ECM scaffold highly mimics the complex morphology and composition of natural ECM, and can be engineered to display different topography and composition [16, 17]. We have recently derived a highly aligned ECM scaffold from a human dermal fibroblast cell sheet grown on nanograted substrate [18]. The ECM scaffold contains aligned protein nanofibers of 78 ± 9 nm in diameter, which is comparable to the collagen nanofiber size in human body, and support the cell growth and alignment [18]. The aligned ECM scaffold also replicates the anisotropic architecture found in many native tissues such as blood vessel and myocardium. Our ECM scaffold is mainly composed of polypeptides with numerous primary amine groups which enable conjugation of NO donors through carboxylic acid reaction [19]. S-Nitroso-N-acetyl-D-penicillamine (SNAP) is one of the well-known biocompatible NO donors that naturally releases NO under physiological conditions. In this study, SNAP was incorporated into the aligned ECM scaffold for localized NO release.

Human mesenchymal stem cells (hMSCs) exist in virtually all tissues in the body including bone marrow, fat, muscle, and skin. Several studies suggest that hMSCs contribute to tissue regeneration after mobilization, migration and engraftment of the damaged tissues [20–22]. The immune cells, inflammatory cytokines together with fibroblasts and endothelial cells in the wound area release signals recuiting hMSCs to migrate into the stroma of the damaged tissues. Then hMSCs differentiate into corresponding cell types, as well as release various growth factors and chemokines promoting tissue regeneration and repair [22]. In addition, systematically administrated MSCs can also migrate toward specific tissues to improve tissue regeneration [23]. Therefore, the *in vitro* investigation of the response of hMSCs to NO in an interactive ECM scaffold model will contribute to the current understanding of the extremely complex tissue healing mechanism.

In the present work, a highly aligned natural ECM scaffold capable of releasing NO was fabricated to provide an ECM-rich microenvironment partially mimicking the *in vivo* stroma in wound healing site. The effects of locally released NO on hMSCs' viability, proliferation, morphology, and adhesion were studied. The results will provide new insights into the mechanism of NO therapeutics in wound healing by studying the cellular response to exogenously delivered NO.

Materials and Methods

Preparation of highly aligned ECM scaffold

The fabrication of highly aligned ECM scaffold followed our previously published paper [24]. Briefly, the nano-grated Polydimethylsiloxane (PDMS) was coated with bovine collagen I to facilitate cell adhesion. Human dermal fibroblasts (ATCC, Manasass, VA) at passage 4 were seeded on the PDMS at a density of 10,000 cells cm^{-2}. The cells were cultured in Dulbecco's Modified Eagle Medium (DMEM) supplemented with 20% fetal bovine serum (FBS), 20% Ham F12, 500 μM sodium ascorbate, and 1% penicillin/streptomycin (Life Technologies, Rockville, MD). The culture was maintained by changing medium twice per week and cells were allowed to proliferate for up to 6 weeks. The resulting fibroblast cell sheet was placed into the first decellularization solution, which contained 1 M NaCl, 10 mM Tris, and 5 mM Ethylenediaminetetraacetic acid (EDTA) (Sigma, St Louis, MO). The cell sheet was shaken for 1 h at room temperature and rinsed thoroughly with phosphate buffered saline (PBS). The cell sheet was then placed in a second decellularization solution containing 0.5 wt% SDS, 10 mM Tris, and 5 mM EDTA, and shaken for 0.5 h at room temperature. After PBS wash, the sample was rinsed in DMEM medium with 20% FBS for 48 h at room temperature and rinsed again with PBS.

Preparation of SNAP incorporated ECM scaffold

The ECM scaffolds were sterilized with 70% ethanol and rinsed with PBS. Then the ECM scaffold was soaked in a mixture of N-Ethyl-N′-(3-dimethylaminopropyl)carbodiimide (EDC) (5 mM, Sigma) and SNAP (1mM, Sigma) solution in DI H_2O at 4 °C for 18 h. The EDC-SNAP solution was removed and the scaffold was washed with DI H_2O and ready for cell seeding. The SNAP incorporated ECM scaffold was designated as SNAP-ECM, and the ECM scaffold without modification was designated as control ECM.

Chemical structure and morphology of the ECM scaffold

The chemical structure of the ECM scaffold was observed with an attenuated total reflectance-infrared spectroscopy (FTIR-ATR). The dried samples were frozen in liquid nitrogen for 10 seconds, crushed into small pieces with a mortar and pestle, and then analyzed following the instrument's standard operating procedures. For morphology observation, samples were fixed with 4% paraformaldehyde, dehydrated, and sputter-coated with a 5 nm platinum coating. The morphology of the ECM scaffolds was viewed by a Hitachi S-4700 FE-SEM.

NO release profile

The NO release under physiological conditions was measured as described in our previous publication [25]. To do this, the samples were immersed in cell culture medium at 37 °C in 5% CO_2 incubator. The supernatant was collected at specific time points for nitrite concentration quantification via the Griess assay kit (Life Technologies) with absorbance recorded on a Versamax tunable microplate reader (Molecular Devices, Sunnyvale, CA).

hMSCs culture, viability, apoptosis and proliferation assay

Bone marrow–derived hMSCs were provided by Texas A&M University Health Science Center. Passage 5 hMSCs were seeded on SNAP-ECM and control ECM at the density of 7,000 cells/cm^2 and cultured in alpha-MEM supplemented with 10% FBS, 1% L-glutamine, and 1% penicillin/streptomycin (Life Technologies). Samples were taken out at 6h and 24h, and viable cells were stained by calcein AM (Life Technologies) and counted. Another set of samples were harvested for apoptosis assay using EnzChek® Caspase-3 Assay Kit #2 (Life Technologies). For proliferation assay, samples were taken out at 24 h and 72 h, fixed and stained with Ki67 and DAPI. The percentage of Ki67-positive cells was calculated as the number of Ki67-positive cells divided by the total number of cells obtained from DAPI staining, and the data was pooled for statistical analysis.

Cytoskeleton protein and adhesion molecule staining and quantification

Samples were taken out at 6 and 24 h, fixed with 4% paraformaldehyde, blocked with 1% bovine serum albumin, and incubated with primary antibodies against integrin $\alpha5$ and paxillin (Abcam, Cambridge, MA). The samples were then washed and incubated with secondary antibodies conjugated to Alexa Fluor 488 (Life Technologies). The F-actin was stained with rodamine phalloidin (Life Technologies). Finally the samples were mounted and viewed using an Olympus FV-1000 confocal microscope or Olympus BX-51 fluorescent microscope. All the images were taken at the identical settings. The intensity of integrin $\alpha5$

and paxillin in each cell was analyzed by Image J using the previously published method [26]. The mean level of intensity was obtained by dividing total fluorescence intensity by cell area for at least 20 cells in each condition.

Statistics/data analysis

Experiment results were expressed as means ± standard deviation (SD) of the means of the samples (at least three independent samples were used for each assay). Student's t-test (Microsoft Excel) was used for comparisons, and statistical significance was accepted at $p < 0.05$.

Results

Chemical modification of the ECM scaffolds

The reaction scheme for preparing SNAP-ECM was demonstrated in Scheme 1. The primary amine groups on protein chains in the ECM scaffold reacted with the carbonyl groups on SNAP, with the aid of crosslinking reagent EDC, resulting in amide bond formation. Figure 1 showed the FTIR-ATR spectra of the ECM scaffolds before and after SNAP functionalization. The characteristic bands of the protein structure were the C=O stretching for amide I at around 1628 cm^{-1}, N-H deformation for amide II at around 1540 cm^{-1}, C-N stretching for amide II at around 1400 cm^{-1}, and N-H bending for amide III at around 1236 cm^{-1}. The 1540 cm^{-1} peak shifted to 1553 cm^{-1} after SNAP-incorporation, which might indicate the conjugation of SNAP molecules into the protein. The overall peak position and intensity did not change significantly, suggesting that the incorporation of SNAP did not affect the basic ECM chemical structure.

Morphology and NO-releasing of the ECM scaffolds

The SEM images in Figure 2 revealed that the ECM scaffolds contained numerous ECM protein nanofibers, most of which were aligned in the same direction. After SNAP-conjugation, the nanofibers in the ECM scaffold maintained their morphology and alignment.

The NO release profile from the SNAP-ECM and control ECM scaffolds within 72 hours under physiological conditions was depicted in Figure 2 C and D. The cumulative NO release was characterized with a rapid NO generation within the first two hours and a much slower release rate in the remaining time. From 24 h to 72 h, the increase of NO concentration was quite low. During the continuous 72 h of NO release, the *in situ* NO concentration rose from around 6.2 μM to 16.2 μM. On the contrary, the control-ECM did not show any detectable NO release over the 72 h period.

Cell viability, apoptosis, and proliferation

The viable cell number per area was counted and shown in Figure 3A. At 6 h, the viable cells on SNAP-ECM and control ECM were comparable (15.0 ± 0.7 cells/mm^2 for SNAP-ECM verses 15.7 ± 0.7 cells/ mm^2 for control-ECM). After 24 h of continuous exposure to NO, the number of viable cells on SNAP-ECM slightly decreased to 14.6 ± 0.7 cells /mm^2, which was significantly lower than that on the control ECM (20.0 ± 0.3 cells/mm^2)

(p<0.01). The apoptosis assay in Figure 3B indicated that there were more apoptotic cells on SNAP-ECM than on control ECM. The significant difference was only found at 6 h (p<0.05). The apoptotic cells increased on both scaffolds from 6 h to 24 h. The proliferation of hMSCs was analyzed by Ki67 expression, as shown in Figure 3C. The average percentage of Ki67 positive cells on SNAP-ECM decreased from 41.8 ± 2.4% at 24 h to 26.9 ± 2.8% at 72 h. On the other hand, the percentage of Ki67 positive cells on control-ECM increased from 33.6 ± 0.6% at 24 h to 48.2 ± 4.0 % at 72 h. There were significant difference between SNAP-ECM and control-ECM at both time points (p<0.01).

Morphology and cytoskeleton organization in hMSCs

The morphology of hMSCs grown on SNAP-ECM and control-ECM was quite different as observed in the SEM images of Figure 4 A. Most of the cells on SNAP-ECM exhibited round and retracted cell body with less filopodia; while most of the cells on control ECM had stretched and elongated cell body with more filopodia. The morphology difference was also confirmed by cytoskeleton protein F-actin staining (Figure 4 B). After 6 h attachment on the control ECM scaffold, the F-actin fibers in most of hMSCs exhibited very good orientation along one direction, which was arisen by the directional clue of underlying highly aligned ECM fibers. On the contrary, the F-actin fibers of hMSCs grown on SNAP-ECM were randomly distributed throughout the cells. At 24 h, the F-actin in hMSCs on the control ECM remained highly aligned, and the F-actin organization in MSCs on SNAP-ECM was still in disorder. The mean area of each cell on SNAP-ECM was significantly smaller than the mean area covered by a cell on control-ECM at both 6 h and 24 h (Figure 5 A). In addition, from 6 h to 24 h the mean cell area increased 12% for control-ECM sample, but only increased less than 1% for SNAP-ECM sample. The circularity of cells grown on SNAP-ECM was consistently higher (p< 0.01) than those cells on control-ECM at both times points (Figure 5 B), which quantitatively revealed that cells on SNAP-ECM exhibited more polygonal or rounder morphology than cells on control-ECM. From 6 h to 24 h, the circularity of cells decreased 8% and 22% for SNAP-ECM and control-ECM samples, respectively. The circularity reduction indicated that hMSCs started to elongate on both samples, but became much more stretched on control-ECM.

Adhesion molecules expression

The focal adhesion related molecules, including paxillin and integrin α5, expressed in hMSCs on control ECM and SNAP-ECM were stained and quantified, as shown in Figure 6. The cells grown on the control ECM exhibited positive staining not only around the nucleus, but also at the edge of stretched cell body. Although the cells grown on SNAP-ECM did not spread as much as the control, the α5 and paxillin staining appeared throughout the cell surface. The image quantification showed that both paxillin and α5 intensity in cells grown on SNAP-ECM was significantly lower than that on the control ECM throughout 24 h except that the α5 intensity on SNAP-ECM at 24 h was not statistically different than the corresponding control.

Discussion

The influence of NO on cell proliferation, migration and differentiation have been studied using different NO donors on various substrates such as tissue culture plastic, hydrogel and polymer nanofibers [25, 27, 28]. However, none of these systems provide a naturally occurring ECM-rich microenvironment that can dynamically interact with cells and mediating molecules involved in tissue healing process. Highly aligned cell-derived ECM scaffolds recapitulate both the *in vivo* 3D nanofibrous anisotropic structure and biochemical microenvironment, therefore can serve as an ideal platform to study the *in vitro* cell growth, adhesion and interaction. In this work, the ECM scaffold was employed not only to support cell culture but also to deliver locally released NO after SNAP conjugation. Our study demonstrated the NO (with concentration at micro-molar level) can significantly impact the hMSC proliferation, morphology, and adhesion, on the ECM scaffold.

The capacity of NO to regulate cell proliferation varies depending on NO concentration and cell types. It has been reported that low doses of NO can promote endothelial cell growth but induce apoptosis and senescence in smooth muscle cell and fibroblasts [3, 29]. High doses of NO has inhibitory effects on all cells. The NO level measured in the wound fluid of miscellaneous wounds was reported largely in the range of 5 to 100 μM [30]. In our experiment, the NO concentration at 6 h was around 9.7 μM and increased to around 15.5 μM at 24 h, which was within the reported physiological NO range. The initial exponential increase of NO also resembled the rapid accumulation of NO in the early inflammation phase. In the following 48 hours, the NO concentration only increased 0.7 μM. Thus, most of our cellular assays were performed within the first 24 hours. The comparable viable hMSCs at 6 h on both SNAP-ECM and the control ECM indicated that this level of NO did not affect the initial cell attachment on the ECM scaffold. However, the NO resulted in the presence of more apoptotic cells, retracted cellular body, and less expression of adhesion molecules. This initial cell inhibitory tendency on SNAP-ECM continued. At 24 h, hMSCs exposed to NO had significantly less viable cells, cell spreading, and focal adhesions molecules. Although there was higher percentage of proliferating hMSCs on SNAP-ECM at 24 h, the proliferation of hMSCs on SNAP-ECM was seriously inhibited by 72h. The overall effect of the NO-releasing ECM scaffold on hMSCs during this period was suppressing. The result was correspondent with previous evidences that NO inhibited proliferation of smooth muscle cells, endothelial cells, and fibroblasts [27, 31]. Due to the fact that different materials and various cell growth assays were used in those reports, it was difficult to compare our results with other studies completely.

The hMSCs on SNAP-ECM showed reduced cellular area and round cell shape, which was consistent with several other studies that the continuous exposure to NO resulted in cellular area reduction and morphology change. The bone marrow MSCs cultured in the presence of 200 μM SNAP showed significant reduction of cellular area [32]. The swiss 3T3 cells without SNAP treatment demonstrated substantial degree of spreading compared to the SNAP-treated cells [33]. Similar results were also found in the renal tubule epithelial cell culture, where the addition of a NO donor produced rapid retraction of lamellipodia together with cell rounding [34]. The underlying mechanism is involved with the stress fiber formation or the status of actin polymerization, which controls the cell shape and lamellipodia protrusion. Our results demonstrated that the cells on the control ECM elongated and the stress fibers (F-actin) stretched and aligned, which corresponded to the lamellipodia protrusion shown in Figure 4 A. While cells on SNAP-ECM had round cell body and the stress fibers were contracted and disoriented, which corresponded to the lamellipodia retraction shown in Figure 4 A. The proliferation and cytoskeleton organization of hMSCs are closely associated with cell phenotype and paracrine signaling [35]. The actin cytoskeleton configuration can be used as one of the indicators for hMSC differentiation. While hMSCs were in the process of differentiation, cell proliferation decreased. The reduction of cell growth and cellular area on SNAP-ECM indicated that in the context of wound healing microenvironment, where NO is present at the micro-molar level, hMSCs may undergo differentiation and functioning through releasing paracrine factors. Several studies demonstrated that MSCs in the wound sites expressed keratinocyte-specific markers, contributed to fibroblasts in fibrotic lesion and formed glandular structure [36, 37]. In addition, MSCs secreted pro-angiogenic factors to promote formation of new capillary tubes in the wound site [36].

The NO-releasing scaffold also influenced the focal adhesion of hMSC as shown by the expression of integrin $\alpha5$ and the focal adhesion adapter protein paxillin. Focal adhesions usually appear at the edge of cells, which sense environmental cues. The organization of focal adhesions affects many cellular events including cell survival, migration and differentiation [38]. The *N*-terminal of paxillin can bind to the regulator of actin organization. Integrin $\alpha5$ connects ECM protein fibronectin and cytoskeleton protein F-actin through adaptor proteins. In this study, we found that the increased randomness of F-actin was concurrent with the relatively lower expression of paxillin and integrin $\alpha5$ for cells grown on SNAP-ECM. The observation was consistent with previous reports that the NO may play a role in destabilization of contacts between focal adhesion and the cytoskeleton, thus releasing cytoskeleton from the focal adhesion complex [39]. Another study also showed that NO inhibited adhesion of human umbilical vein endothelial cells (HUVECs) and attenuated recruitment of paxillin [28]. There was a strong dependence on integrin $\alpha5$ of cell attachment, proliferation and migration in 3D cell derived ECM [40]. The decreased α_5 expression in our study was also correspondent to the less viable and proliferating cells on SNAP-ECM. It was reported that the effect of NO on actin stress fiber formation is time-dependent and reversible [34]. We also found that the expression of α_5 and paxillin slightly increased from 6 to 24 h for SNAP-ECM samples. In addition, the NO-exposed cells had a tendency to elongate with time increasing after 24 h. Collectively, all the data indicated that the effect of NO on cell morphology, adhesion, and migration may slowly diminish when NO releasing rate is decreased. It was reported that the co-localization pattern of integrin $\alpha5$, paxillin and fibronectin on 3D cell derived ECM was similar to the pattern observed *in vivo*, which was probably due to the similarity of composition or 3D structure [40]. Therefore, the results obtained in our experiments may reflect the cell adhesion patterns found in the body. During wound healing process, the expression of focal adhesion molecules is critical for cell migration on the surrounding ECM as well as the cell response to growth factors [2]. For example, integrin $\alpha5$ is a major receptor for fibronectin that acts as provisional matrix, allowing for epithelial cell attachment and migration across the wounds [41]. The reduced expression of focal adhesion molecules indicated the possible restricted hMSC mobility in the initial inflammatory phase of wound healing. The hMSCs retained in the wound area may benefit the tissue healing.

Conclusions

Here we reported the effects of locally delivered NO on the viability, morphology, and adhesion of hMSCs grown on a SNAP-incorporated natural ECM scaffold. The NO-releasing scaffold provided an *in vitro* platform that partially mimics the *in vivo* stromal microenvironment in wound healing. The results showed that the presence of micro-molar level of NO in SNAP-ECM led to lower cell viability and decreased proliferation, which was consistent with reduced cellular area and disrupted organization of F-actin stress fibers. The decreased expression of focal adhesion related molecules integrin α5 and paxillin implied that the cell migration would be suppressed. These results may contribute to our knowledge of hMSC behaviors in a NO-rich environment during wound healing process.

Acknowledgments

This study was supported by the National Institutes of Health (1R15HL115521-01A1) and the Research Excellence Fund-Research Seed Grant (REF-RS) from Michigan Technological University to F.Z. The authors wish to thank Caleb Vogt in our research group for his help in drawing graphic illustration of SNAP-ECM reaction scheme (scheme 1). The authors also wish to thank Mitchell Tahtinen in our group for helpful suggestions on the writing of manuscript.

References

1. Broughton G, Janis JE, Attinger CE. The basic science of wound healing. Plastic and Reconstructive Surgery. 2006; 117:12S–34S. [PubMed: 16799372]
2. Schultz GS, Wysocki A. Interactions between extracellular matrix and growth factors in wound healing. Wound Repair and Regeneration. 2009; 17:153–62. [PubMed: 19320882]
3. Schwentker A, Billiar TR. Nitric oxide and wound repair. Surgical Clinics of North America. 2003; 83:521. [PubMed: 12822723]
4. Wink DA, Hines HB, Cheng RYS, Switzer CH, Flores-Santana W, Vitek MP, et al. Nitric oxide and redox mechanisms in the immune response. J Leukocyte Biol. 2011; 89:873–91. [PubMed: 21233414]
5. Dattilo JB, Makhoul RG. The role of nitric oxide in vascular biology and pathobiology. Annals of Vascular Surgery. 1997; 11:307–14. [PubMed: 9140609]
6. Bernatchez SF, Menon V, Stoffel J, Walters S-AH, Lindroos WE, Crossland MC, et al. Nitric oxide levels in wound fluid may reflect the healing trajectory. Wound Repair and Regeneration. 2013; 21:410–7. [PubMed: 23627618]
7. Witte MB, Barbul A. Role of nitric oxide in wound repair. American Journal of Surgery. 2002; 183:406–12. [PubMed: 11975928]
8. Ignarro, LJ. Nitric Oxide: Biology and Pathobiology. San Diego: Academic Press; 2000.
9. Riccio DA, Schoenfisch MH. Nitric oxide release: Part I. Macromolecular scaffolds. Chemical Society Reviews. 2012; 41:3731–41. [PubMed: 22362355]
10. Daley WP, Peters SB, Larsen M. Extracellular matrix dynamics in development and regenerative medicine. J Cell Sci. 2008; 121:255–64. [PubMed: 18216330]
11. Badylak SF, Freytes DO, Gilbert TW. Extracellular matrix as a biological scaffold material: Structure and function. Acta Biomater. 2009; 5:1–13. [PubMed: 18938117]
12. John, M.; McPherson, KAP. Collagen in dermal wound repair. New York: Plenum Press; 1988.
13. Clark RAF. FIBRONECTIN MATRIX DEPOSITION AND FIBRONECTIN RECEPTOR EXPRESSION IN HEALING AND NORMAL SKIN. Journal of Investigative Dermatology. 1990; 94:S128–S34.

14. Peplow PV. Glycosaminoglycan: a candidate to stimulate the repair of chronic wounds. Thrombosis and Haemostasis. 2005; 94:4–16. [PubMed: 16113778]
15. Muller M, Trocme C, Lardy B, Morel F, Halimi S, Benhamou PY. Matrix metalloproteinases and diabetic foot ulcers: the ratio of MMP-1 to TIMP-1 is a predictor of wound healing. Diabetic Medicine. 2008; 25:419–26. [PubMed: 18387077]
16. Petrie RJ, Gavara N, Chadwick RS, Yamada KM. Nonpolarized signaling reveals two distinct modes of 3D cell migration. J Cell Biol. 2012; 197:439–55. [PubMed: 22547408]
17. Goetz JG, Minguet S, Navarro-Lerida I, Lazcano JJ, Samaniego R, Calvo E, et al. Biomechanical Remodeling of the Microenvironment by Stromal Caveolin-1 Favors Tumor Invasion and Metastasis. Cell. 2011; 146:148–63. [PubMed: 21729786]
18. Xing Q, Vogt C, Leong KW, Zhao F. Highly Aligned Nanofibrous Scaffold Derived from Decellularized Human Fibroblasts. Advanced Functional Materials. 2014; 24:3027–35. [PubMed: 25484849]
19. Reynolds MM, Frost MC, Meyerhoff ME. Nitric oxide-releasing hydrophobic polymers: Preparation, characterization, and potential biomedical applications. Free Radical Biol Med. 2004; 37:926–36. [PubMed: 15336308]
20. Neuss S, Becher E, Woltje M, Tietze L, Jahnen-Dechent W. Functional expression of HGF and HGF receptor/c-met in adult human mesenchymal stem cells suggests a role in cell mobilization, tissue repair, and wound healing. Stem Cells. 2004; 22:405–14. [PubMed: 15153617]
21. Horwitz EM, Prockop DJ, Fitzpatrick LA, Koo WWK, Gordon PL, Neel M, et al. Transplantability and therapeutic effects of bone marrow-derived mesenchymal cells in children with osteogenesis imperfecta. Nat Med. 1999; 5:309–13. [PubMed: 10086387]
22. Kawada H, Fujita J, Kinjo K, Matsuzaki Y, Tsuma M, Miyatake H, et al. Nonhematopoletic mesenchymal stem cells can be mobilized and differentiate into cardiomyocytes after myocardial infarction. Blood. 2004; 104:3581–7. [PubMed: 15297308]
23. Chen JL, Li Y, Wang L, Zhang ZG, Lu DY, Lu M, et al. Therapeutic benefit of intravenous administration of bone marrow stromal cells after cerebral ischemia in rats. Stroke. 2001; 32:1005–11. [PubMed: 11283404]
24. Xing Q, Yates K, Tahitnen M, Shearier EZQ, Zhao F. Decellularization of fibroblast cell sheets for natural extracellular matrix scaffold preparation. Tissue Engineering Part C: Methods. 2014
25. Xing Q, Yates K, Bailey A, Vogt C, He W, Frost MC, et al. Effects of local nitric oxide release on human mesenchymal stem cell attachment and proliferation on gelatin hydrogel surface. Surface Innovations. 2013; 1:224–32.
26. Shi F, Sottile J. Caveolin-1-dependent beta 1 integrin endocytosis is a critical regulator of fibronectin turnover. J Cell Sci. 2008; 121:2360–71. [PubMed: 18577581]
27. Yu H, Payne TJ, Mohanty DK. Effects of Slow, Sustained, and Rate-Tunable Nitric Oxide Donors on Human Aortic Smooth Muscle Cells Proliferation. Chemical Biology & Drug Design. 2011; 78:527–34. [PubMed: 21740530]
28. Kushwaha M, Anderson JM, Bosworth CA, Andukuri A, Minor WP, Lancaster JR, et al. A nitric oxide releasing, self assembled peptide amphiphile matrix that mimics native endothelium for coating implantable cardiovascular devices. Biomaterials. 2010; 31:1502–8. [PubMed: 19913295]
29. Garg UC, Hassid A. NITRIC OXIDE-GENERATING VASODILATORS AND 8-BROMO-CYCLIC GUANOSINE-MONOPHOSPHATE INHIBIT MITOGENESIS AND PROLIFERATION OF CULTURED RAT VASCULAR SMOOTH-MUSCLE CELLS. J Clin Invest. 1989; 83:1774–7. [PubMed: 2540223]
30. Bernatchez SF, Menon V, Stoffel J, Walters SAH, Lindroos WE, Crossland MC, et al. Nitric oxide levels in wound fluid may reflect the healing trajectory. Wound Repair and Regeneration. 2013; 21:410–7. [PubMed: 23627618]
31. Nishio E, Fukushima K, Shiozaki M, Watanabe Y. Nitric oxide donor SNAP induces apoptosis in smooth muscle cells through cGMP-independent mechanism. Biochemical and Biophysical Research Communications. 1996; 221:163–8. [PubMed: 8660329]
32. Fuseler JW, Valarmathi MT. Modulation of the migration and differentiation potential of adult bone marrow stromal stem cells by nitric oxide. Biomaterials. 2012; 33:1032–43. [PubMed: 22071099]

33. Sosroseno W, Sugiatno E, Samsudin AR, Ibrahim MF. The effect of nitric oxide on the production of cyclic AMP by a human osteoblast (HOS) cell line stimulated with hydroxyapatite. Biomedicine & Pharmacotherapy. 2008; 62:328–32. [PubMed: 17988826]

34. Lindsay SL, Ramsey S, Aitchison M, Renne T, Evans TJ. Modulation of lamellipodial structure and dynamics by NO-dependent phosphorylation of VASP Ser239. J Cell Sci. 2007; 120:3011–21. [PubMed: 17684063]

35. Mathieu PS, Loboa EG. Cytoskeletal and Focal Adhesion Influences on Mesenchymal Stem Cell Shape, Mechanical Properties, and Differentiation Down Osteogenic, Adipogenic, and Chondrogenic Pathways. Tissue Engineering Part B-Reviews. 2012; 18:436–44. [PubMed: 22741572]

36. Wu Y, Chen L, Scott PG, Tredget EE. Mesenchymal stem cells enhance wound healing through differentiation and angiogenesis. Stem Cells. 2007; 25:2648–59. [PubMed: 17615264]

37. Wu Y, Wang J, Scott PG, Tredget EE. Bone marrow-derived stem cells in wound healing: a review. Wound Repair and Regeneration. 2007; 15:S18–S26. [PubMed: 17727462]

38. Charras G, Sahai E. Physical influences of the extracellular environment on cell migration. Nature Reviews Molecular Cell Biology. 2014; 15:813–24. [PubMed: 25355506]

39. Monteiro HP, Silva EF, Stern A. Nitric oxide: a potential inducer of adhesion-related apoptosis-anoikis. Nitric Oxide-Biology and Chemistry. 2004; 10:1–10.

40. Cukierman E, Pankov R, Stevens DR, Yamada KM. Taking cell-matrix adhesions to the third dimension. Science. 2001; 294:1708–12. [PubMed: 11721053]

41. Carter RT. The role of integrins in corneal wound healing. Veterinary Ophthalmology. 2009; 12:2–9. [PubMed: 19891645]

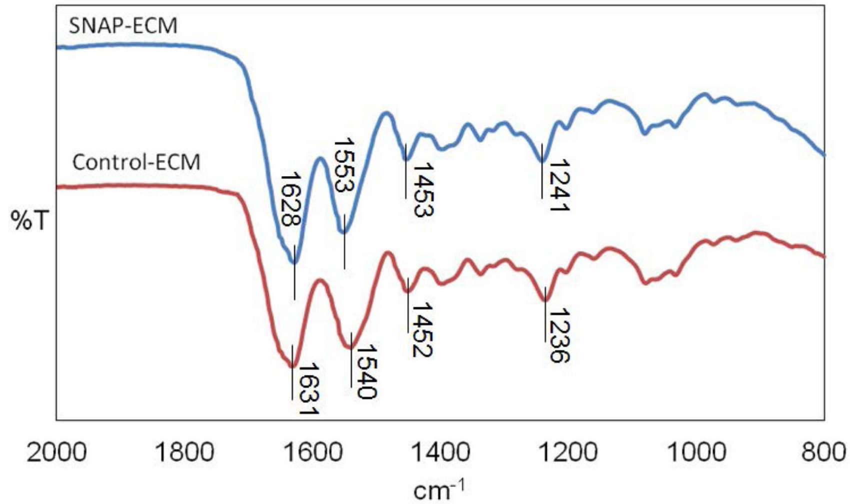

Figure 1.

FTIR spectrum of SNAP-ECM and control ECM. The 1540 cm^{-1} peak shifted to 1553 cm^{-1} after the reaction while the overall peak position and intensity did not change significantly, indicating the SNAP molecules were conjugated into the proteins but did not affect their basic ECM chemical structure.

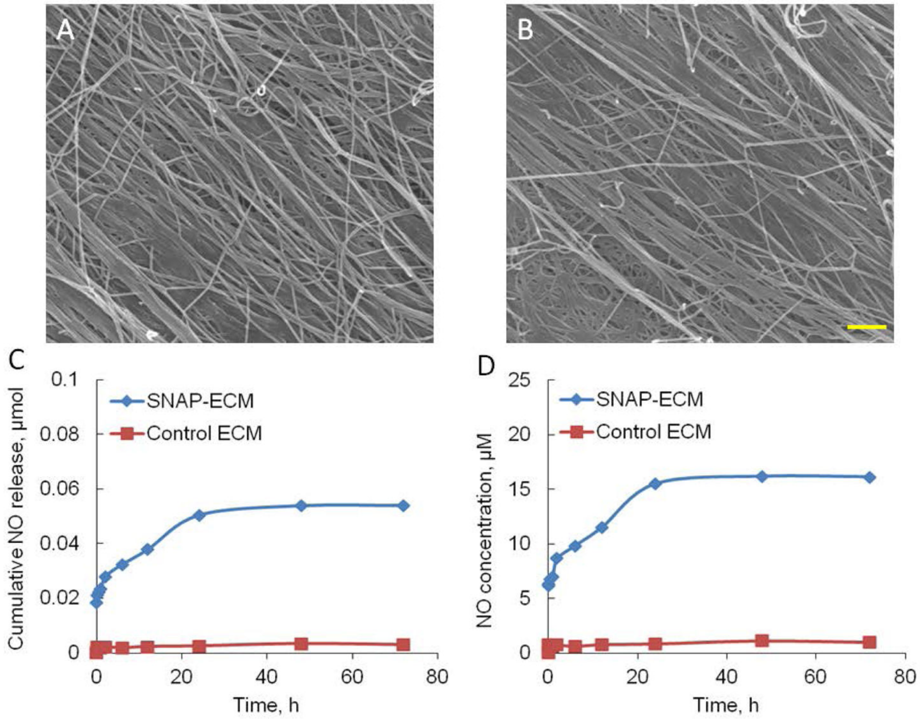

Figure 2.

Morphology and NO release profile of SNAP-ECM and control ECM. (A) SEM image of SNAP-ECM; (B) SEM image of control ECM; scale bar: 1 µm. (C) The cumulative NO release and (D) NO concentration over 72 h from SNAP-ECM and control ECM under physiological conditions. The ECM scaffold morphology did not change significantly after SNAP incorporation. The SNAP-ECM scaffold showed continuous NO release over 72 h.

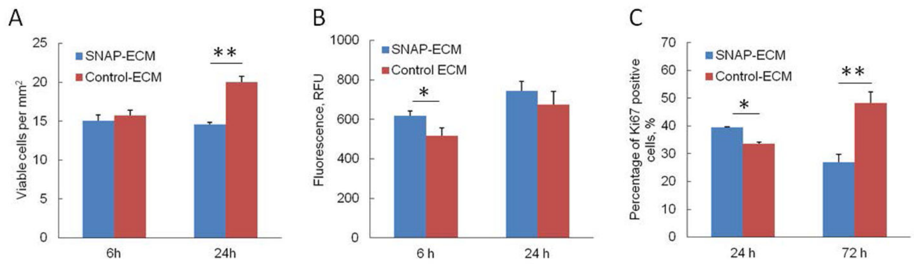

Figure 3.

Culture of hMSCs on SNAP-ECM and control ECM. (A) Viability, (B) apoptosis and (C) proliferation of hMSCs. The cells on SNAP-ECM showed less viability by 24 h and less proliferation capacity by 72 h than those on normal ECM substrates. * $p < 0.05$; ** $p < 0.01$.

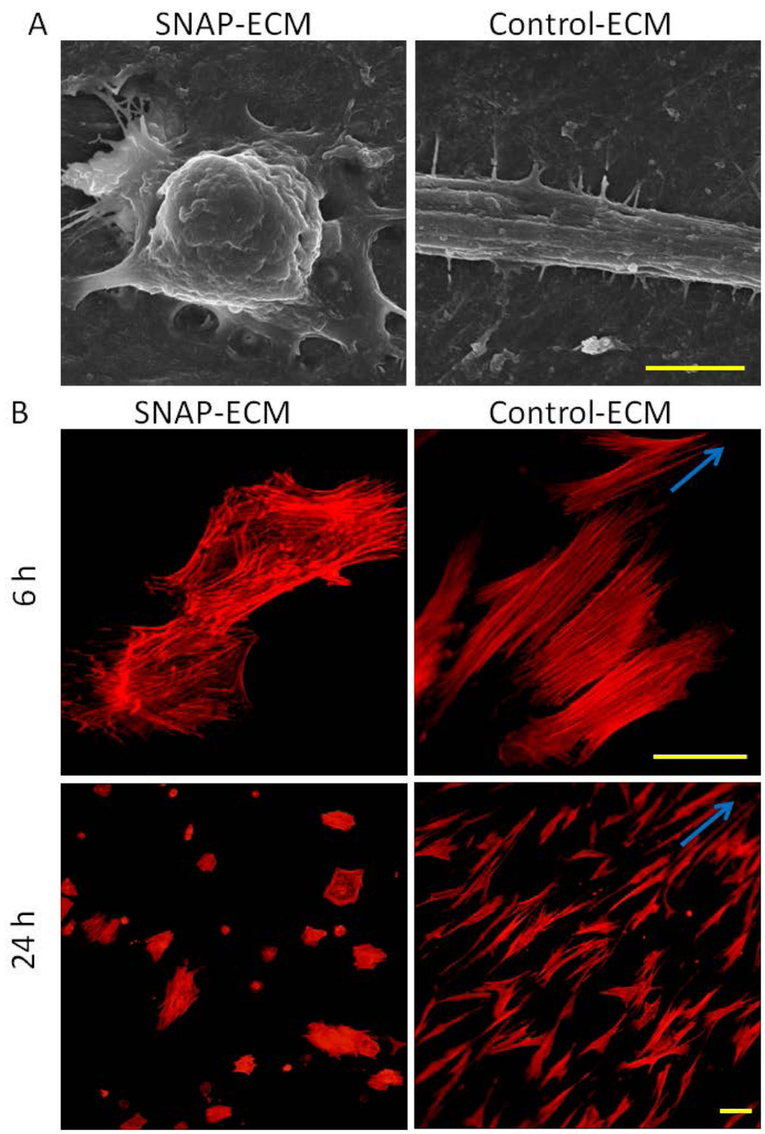

Figure 4.

Morphology and cytoskeleton F-actin organization of hMSCs. (A) SEM images of hMSC on SNAP-ECM and control-ECM at 24 h; scale bar: 5 μm. (B) F-actin staining of hMSCs on SNAP-ECM and control-ECM at 6 and 24 h; Scale bar: 50 μm. Arrows indicate the direction of the alignment. Cells on control ECM stretched the cell body and exhibited more organized F-actin filaments than cells on SNAP-ECM.

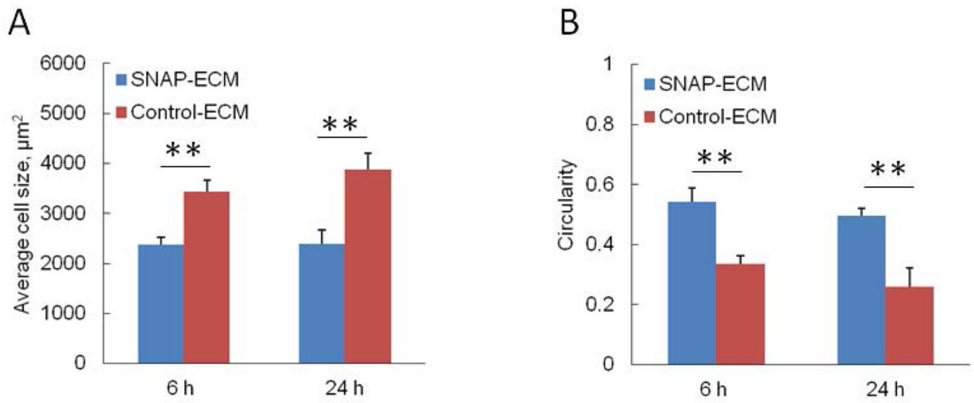

Figure 5.

Quantitative characterization of cell morphology of hMSCs grown on control ECM and SNAP-ECM at 6 and 24 h. (A) Average cellular area covered by each cell; (B) Average circularity of cells. ** $p < 0.01$. Cells on SNAP-ECM covered less area and showed more round shape.

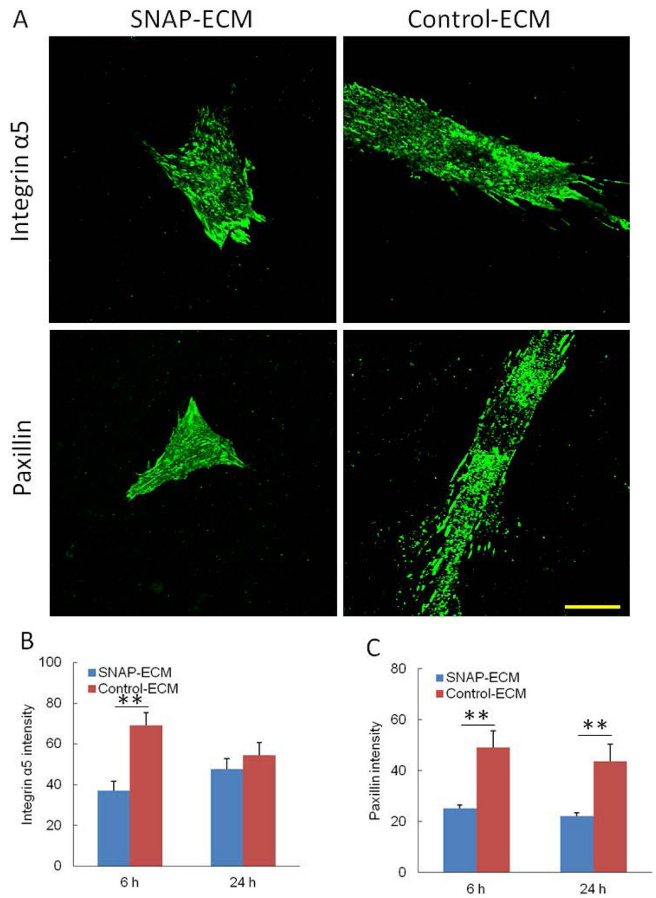

Figure 6.

The expression of focal adhesion related molecules in hMSCs. (A) Immunofluorescence staining of integrin α5 and paxillin on SNAP-ECM and control ECM at 6 h. Scale bar: 40 μm. (B) Intensity of integrin α5 and (C) intensity of paxillin in each cell. ** $p < 0.01$

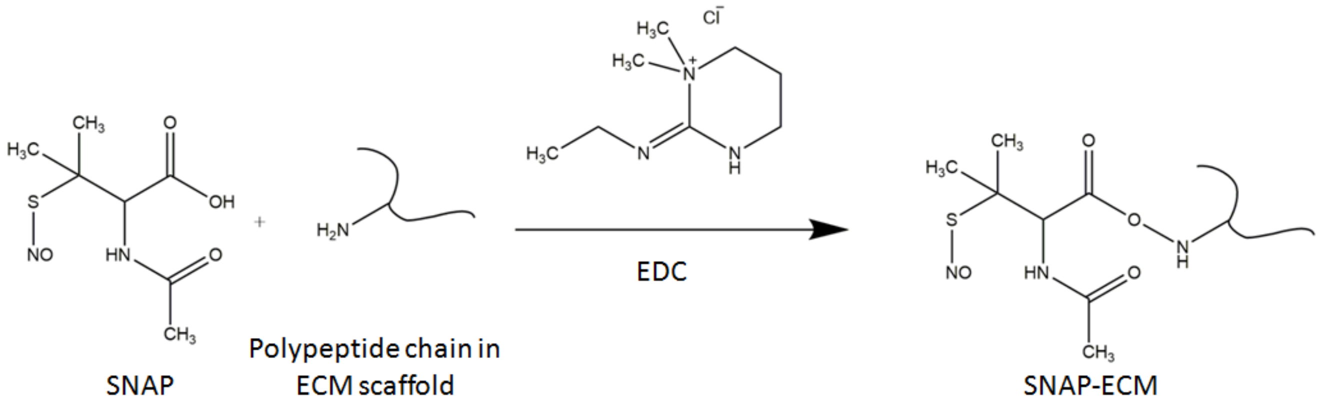

Scheme 1.
The reaction between SNAP and ECM with the aid of crosslinker EDC.